AIAA JOURNAL
Vol. 34, No. 4, April 1996

Nonclassical Effects on Divergence and Flutter of Anisotropic Swept Aircraft Wings

G. Karpouzian*
U.S. Naval Academy, Annapolis, Maryland 21402-5042
and
L. Librescu†
Virginia Polytechnic Institute and State University, Blacksburg, Virginia 24061-0219

A refined structural model of swept aircraft wings is presented and used to study the associated flutter and divergence instability in an incompressible gas flow. The structural model incorporates nonclassical effects such as anisotropy, heterogeneity, transverse shear, and warping inhibition. An exact solution methodology appropriate for parametric studies is used to specifically determine the effects of transverse shear and warping restraint on aeroelastic instabilities. The results reveal strong quantitative and qualitative implications for instability predictions. The solution methodology yields results that are in excellent agreement with an exact approach devised for a special case and provides a high-efficiency mathematical tool for dealing with flutter and divergence instability problems.

Nomenclature

AR	= wing aspect ratio, $2l/c$
a	= dimensionless position of elastic axis, x_o/b
b	= wing semichord length, $c/2$
$C(k)$	= Theodorsen function, $F(k) + iG(k)$
c	= wing chord length measured perpendicular to the reference axis
E	= Young's modulus
G'	= transverse shear modulus
H, H^*	= thickness of wing cross section, H/b
h	= plunging displacement, positive upward
$I^{(m,n)}$	= generalized mass terms
i	= imaginary unit, $\sqrt{-1}$
k	= reduced frequency, $\omega b/V_n$
$\mathcal{L}$	= sectional lift, positive upward, $\mathcal{L}(x_2)$
LT	= Laplace transform operator
l	= wing semispan measured along the reference axis
N	= total number of constituent layers
$Q_{ij}, \bar{Q}_{ij}$	= elastic moduli and their reduced counterparts
Q_n	= normalized dynamic pressure, $q_n c l^3/\bar{D}_{22}$
q_n	= dynamic pressure normal to the reference axis, $(\rho V_n^2/2)$
R	= transverse shear flexibility parameter, E/G'
s	= complex variable for Laplace transform
$\mathcal{T}$	= sectional aerodynamic torque about the elastic axis, positive nose up, $\mathcal{T}(x_2)$
$T_{ij}^{(m,n)}$	= generalized stress couples of $\mathcal{O}(m, n)$, Eq. (8)
t	= time variable
u_1, u_2, u_3	= displacement components of the points of the reference plane
X	= flutter frequency ratio, $(\omega_R/\omega)^2$
x_1, x_2, x_3	= chordwise, spanwise, and transverse normal coordinate to the midplane of the wing, respectively
x_o	= elastic axis position measured from the midchord (positive aft)
Y	= (4×1) vector playing the role of eigenvector
δ	= variation sign
δ_1	= tracer quantity taking the value 1 or 0 depending on whether warping-restraint or free-warping model is considered
η	= dimensionless spanwise coordinate, x_2/l
θ	= twist angle about the pitch axis, positive nose up
Λ	= sweep angle of the reference axis (positive for back swept)
λ_F	= flutter speed parameter, $V_F/b\omega_h$
ν	= Poisson's ratio
ψ_1, ψ_2	= angles of rotation of a line element originally normal to the reference plane about the x_2 and x_1 axes, respectively
Ω_F	= flutter frequency parameter, ω_F/ω_h
ω	= circular frequency of oscillation
ω_R	= reference frequency
$()_{,i}$; $()'$	= $\partial()/\partial x_i$; $\mathrm{d}()/\mathrm{d}\eta$

Introduction

As the concept of high-speed, highly flexible, and light-structural-weight aircraft capable of operating in a very hostile flight environment gathers more impetus, the specialists involved in the development of advanced design methodologies are more and more challenged by new technical problems. Among them, the enhancement of overall aeroelastic behavior and the avoidance of aeroelastic instabilities are of primary concern.

Because of its highly damaging effects, flutter instability must not occur within the operating-flight-speed range of the vehicle. The same is true of divergence instability of forward-swept-wing aircraft and modern fighters.[1] For this reason, accurate stability prediction and improvement of aeroelastic response in the subcritical flight range become imperative.

Of great promise toward the solution of some technical challenges raised by the design of a new generation of highly flexible space vehicles is the ongoing integration in their construction of advanced composite materials. In this sense, a great deal of research activity on aeroelasticity, in general, and on divergence and flutter instabilities, in particular, has been prompted by the adoption of composite material systems in aircraft design.[2–14]

As was revealed conclusively, aeronautical structures constructed of advanced composite materials can experience aeroelastic response behaviors quite different from their standard metallic counterparts.

Two such examples are worthy of mentioning, namely, 1) the static behavior of forward-swept-wing aircraft and 2) the effect of warping restraint (WR) on the static and dynamic behavior of aircraft wings. For case 1, it is well known that incorporation of composite material systems in the design of aircraft wings has the

Presented as Paper 93-1535 at the AIAA 34th Structures, Structural Dynamics, and Materials Conference, La Jolla, CA, April 19–21, 1993; received May 18, 1995; revision received Nov. 10, 1995; accepted for publication Nov. 14, 1995.

*Associate Professor, Department of Aerospace Engineering.
†Professor, Department of Engineering Science and Mechanics.

potential not only of enhancing the static aeroelastic behavior of the aircraft, but also of removing completely from their flight envelope the static aeroelastic instability occuring, in the case of metallic wing aircraft, at very low flight speeds.[3–5,7,10–13] In case 2 the effect of WR on metallic structures is significant only for low-aspect-ratio wing, and St. Venant's torsion theory (implying the discard of warping inhibition) is fairly accurate for moderate- to high-aspect-ratio wings.[15] In contrast, because of the elastic couplings involved, the WR for composite wing structures can extend its effects to high-aspect-ratio wing planforms as well. Moreover, because of the same couplings,[10–12,16,17] adoption of the free-warping (FW) model (i.e., St. Venant's torsion theory) can lead to an unstable design.

These two cases show clearly that the exotic properties featured by the new advanced composite materials, and the increasing complexity of structural systems resulting therefrom, render the classic structural models of aircraft lifting surfaces quite obsolete.

Modern aeroelastic analyses of composite structures are carried out in the aircraft industry with the aid of sophisticated computer codes. In spite of their unarguable importance, their use in preliminary aeroelastic design investigations is precluded.

With this in mind, a comprehensive structural model of anisotropic composite aircraft wings encompassing some nonclassical features is presented as well as a powerful flutter/divergence solution methodology particularly suited to parametric investigation.

The dynamic aeroelastic equations of composite aircraft swept wings are presented first. In addition to the inherent anisotropy and heterogeneity of wing structures composed of advanced composite materials, the governing equations also incorporate other nonclassical characteristics that are generated or exacerbated by the use of such composite materials. This is followed by the study of flutter and divergence instabilities and, for this purpose, an exact solution methodology based on the Laplace transform technique is employed.

Finally, the numerical validation results and their implications for assessment of nonclassical effects on the flutter and divergence instabilities of aircraft wings are discussed.

Assumptions in Aerodynamic and Structural Models

The geometric details and the notations related to the wing configuration considered in the present study are illustrated in Fig. 1. The case of forward- or aft-swept aircraft wings is considered in this study.

The wing structure is idealized as a laminated composite plate whose constituent laminae are characterized by different orthotropic angles and different material and thickness properties. The interface plane between the contiguous layers r and $r+1$ (where $1 \leq r < N$) is selected as the reference plane of the composite structure. The points of the reference plane of the wing (defined by $x_3 = 0$) are referred to as a Cartesian system of in-plane coordinates (x_1, x_2), the upward x_3 coordinate being considered perpendicular to the (x_1, x_2) plane. The reference axis x_2 is selected to coincide with the midchord line along the wingspan.

It is assumed that the wing is sufficiently stiff at the root that it behaves as if it were clamped normal to the reference axis. The angle of sweep (considered positive when swept back and negative when swept forward) is measured in the wing planform from the direction normal to the airstream to the reference axis. All geometric and aerodynamic section parameters are based on sections normal to the reference axis.

For the structural wing model, the commonly used assumption of chordwise nondeformability is adopted. This assumption is justified by the fact that the semimonocoque wing structures usually contain transverse stiffening members that are rigid within their own planes.

The expression of the unsteady aerodynamic loads is consistent with that derived by Barmby et al.[18] for the case of an incompressible flowfield and is applicable to swept wings of high- to moderate-aspect ratios.[19]

General Consideration of Kinematics

One of the important features of anisotropic composite material structures is the transverse shear flexibility characteristic.[20] It is measured in terms of the ratio of the in-plane Young's modulus E_1 to the transverse shear modulus G_{13}. In classic structural theories (i.e., Love–Kirchhoff for plates or shells and Euler–Bernoulli for beams), the ratio E_1/G_{13} is assumed to be zero (which is equivalent to postulating that the material exhibits an infinite stiffness in the transverse shear direction), whereas in nonclassical treatments, consistent with the actual material properties, this ratio is different from zero and for some advanced composite materials it can approach values of $\mathcal{O}(100)$.

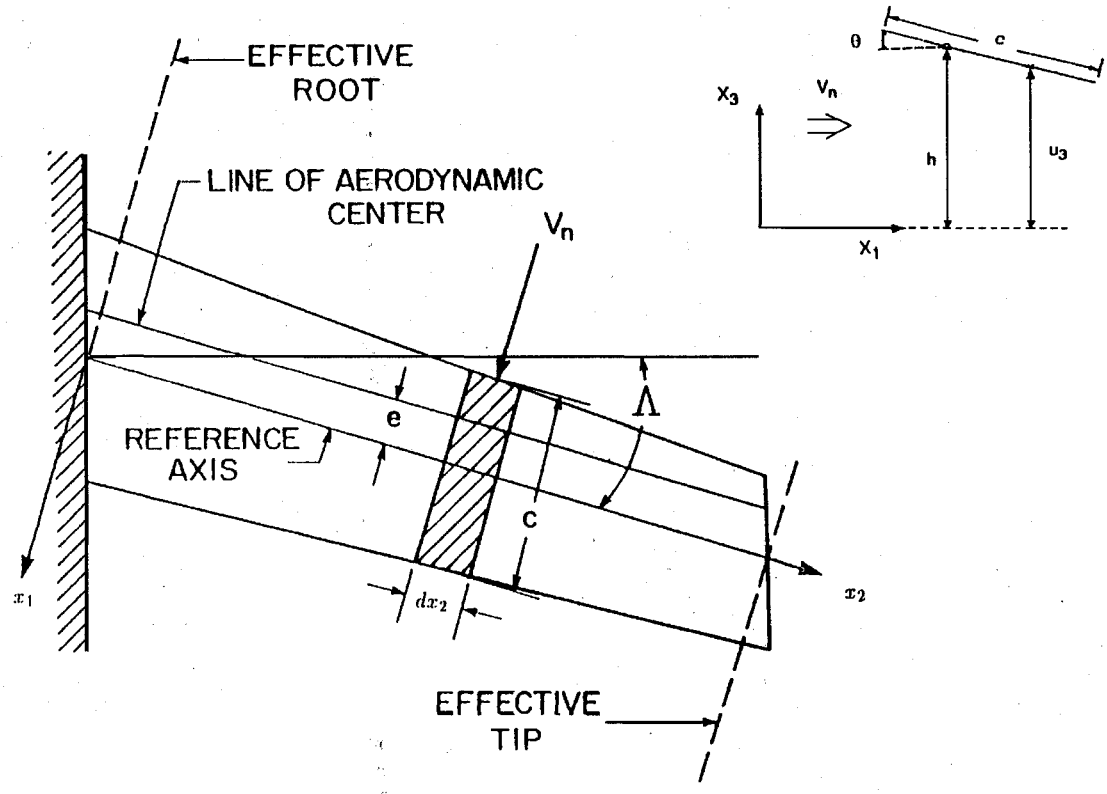

Fig. 1 Geometry of a swept wing (inset: chordwise-rigid plate model).

As emphasized in the subsequent analysis, the neglect of this effect can induce significant quantitative and qualitative errors. Another factor whose effects have not yet been explored, especially in the context of the flutter of aircraft wings, is related to the warping inhibition. Although earlier works have indicated that the FW model provides reasonably accurate predictions except for aircraft wings with fairly low-aspect ratios, these conclusions are based on the assumption that the wing is constructed of isotropic materials.[15] However, recent studies[8] reveal that because of the nonhomogeneous and anisotropic material structures used in modern aircraft, various elastic couplings become prominent and the aerodynamic loads vary significantly along the wingspan; this results in very significant errors when the FW (St. Venant) model is used. Moreover, the St. Venant theory, which has always been shown to provide conservative predictions, can yield nonconservative results.[10–12] Owing to the large errors incurred when the FW wing model is adopted, it becomes clear that the model should be replaced by a more refined one that includes the WR effect.

Having in view that the wing dimensions in the chordwise x_1 and thickness x_3 directions are much smaller than that in the spanwise x_2 direction, the three-dimensional problem can be reduced to an equivalent one-dimensional problem by adopting, as a first step, the following representation of the three-dimensional displacement components:

$$U_1(x_1, x_2, x_3; t) = u_1(x_1, x_2; t) + x_3\psi_1(x_1, x_2; t) \tag{1a}$$

$$U_2(x_1, x_2, x_3; t) = u_2(x_1, x_2; t) + x_3\psi_2(x_1, x_2; t) \tag{1b}$$

$$U_3(x_1, x_2, x_3; t) = u_3(x_1, x_2; t) \tag{1c}$$

Equations (1), well known in the modeling of shear deformable plate and shell theories, correspond to the first-order transverse shear deformation theory (FSDT).[20]

As shown in Ref. 13, consistent with the chordwise-rigid plate model, it follows that $u_1 \to 0, u_2 \to u_2(x_2; t)$, and $\psi_1 \to \psi_1(x_2; t) \equiv \theta(x_2; t)$ where θ is the twist angle of the wing about its pitching axis (positive nose up).

To further reduce the three-dimensional problem of the wing structure to an equivalent one-dimensional one (implying that the wing behavior is adequately defined by a set of functions of a single spanwise x_2 coordinate), we postulate[13]

$$\psi_2(x_1, x_2; t) = \tilde{\psi}_2(x_2; t) + x_1\tilde{\tilde{\psi}}_2(x_2; t) \tag{2a}$$

and

$$u_3(x_1, x_2; t) = h(x_2; t) - (x_1 - x_o)\theta(x_2; t) \tag{2b}$$

Equation (2b) describes the vertical displacement of an arbitrary point along the chordline of a rigid wing cross section (see Fig. 1 inset). Here, $h(x_2; t)$ denotes the plunging displacement of a wing cross section (positive upward) measured at the elastic axis, located at $x_1 = x_o[\equiv x_o(x_2)]$. As a result, Eqs. (1) become

$$U_1 = x_3\theta \tag{3a}$$

$$U_2 = u_2 + x_3(\tilde{\psi}_2 + x_1\tilde{\tilde{\psi}}_2) \tag{3b}$$

$$U_3 = h - (x_1 - x_o)\theta \tag{3c}$$

In conjunction with Eqs. (3), the strain components e_{ij} are

$$e_{11} = U_{1,1} = 0 \tag{4a}$$

$$e_{22} = U_{2,2} = u_{2,2} + x_3(\tilde{\psi}_{2,2} + \delta_1 x_1\tilde{\tilde{\psi}}_{2,2}) \tag{4b}$$

$$\gamma_{12}(\equiv 2e_{12}) = U_{1,2} + U_{2,1} = x_3(\theta_{,2} + \tilde{\tilde{\psi}}_2) \tag{4c}$$

$$e_{33} = U_{3,3} = 0 \tag{4d}$$

$$\gamma_{13}(\equiv 2e_{13}) = U_{1,3} + U_{3,1} = 0 \tag{4e}$$

$$\gamma_{23}(\equiv 2e_{23}) = \tilde{\psi}_2 + x_1\tilde{\tilde{\psi}}_2 + h_{,2} - x_1\theta_{,2} + (x_o\theta)_{,2} \tag{4f}$$

In Eqs. (4) and in the forthcoming developments, $(\,)_{,i} \equiv \partial(\,)/\partial x_i$. Note that δ_1 has been associated with the coefficient of $\tilde{\tilde{\psi}}_{2,2}$ in Eq. (4b) to identify the warping effect. The tracer δ_1 takes the value 1 or 0 according to whether the warping inhibition is incorporated or discarded, respectively.

For $\tilde{\psi}_2 = -h_{,2} - (x_o\theta)_{,2}$ and $\tilde{\tilde{\psi}}_2 = \theta_{,2}$, one obtains $\gamma_{13} = \gamma_{23} = 0$, which is consistent with the traditional assumption of infinite rigidity in transverse shear, a characteristic of metallic wing structures.

One-Dimensional Equations of Motion and Associated Boundary Conditions

Hamilton's variational principle is used to derive the one-dimensional equations of motion and associated boundary conditions. This variational principle can be stated as

$$\delta J = 0; \qquad J \equiv \int_{t_0}^{t_1} (\mathcal{U} - \mathcal{K} + \mathcal{A})\,dt \tag{5}$$

where $\mathcal{U}$, $\mathcal{K}$, and $\mathcal{A}$ denote the strain energy, the kinetic energy, and the potential energy of the body and surface forces, respectively; t_0 and t_1 denote the initial and final times of motion.

From Ref. 20, a more explicit form of Eq. (5) is

$$\delta J = \int_{t_0}^{t_1} dt\left[-\int_\tau \sigma_{ij}\delta U_{i,j}\,d\tau + \int_\tau \gamma(\mathcal{H}_i - \ddot{U}_i)\delta U_i\,d\tau + \int_{\Omega_\sigma} \bar{\sigma}_i\delta U_i\,d\Omega\right] = 0 \tag{6}$$

where the Einstein summation convention and the end conditions $\delta U_i = 0$ at $t = t_0, t_1$ are implied.

In Eq. (6), $\Omega = \Omega_U \cup \Omega_\sigma$ ($\Omega_U \cap \Omega_\sigma = \phi$) is the external boundary of the structure, Ω_U and Ω_σ being its two parts where the displacement and stresses are prescribed, respectively; τ is the volume of the wing structure, $\mathcal{H}_i$ the component of the body force vector $\mathcal{H}$ (per unit mass), σ_{ij} the component of the stress tensor, γ the mass density of the material, the umlaut denotes time derivatives, and an undertilde identifies a prescribed quantity.

Since $d\tau = dA\,dx_2$, where A is the cross-sectional area of the wing, we can express

$$\int_\tau [\cdot]\,d\tau = \int_o^l dx_2 \int_A [\cdot]\,dA \tag{7}$$

Upon defining the one-dimensional generalized stress couples of $\mathcal{O}(m, n)$ (measured per unit span),

$$T_{ij}^{(m,n)}(x_2) = \int_A \sigma_{ij}x_1^m x_3^n\,dA \tag{8}$$

as well as the generalized body forces and mass terms

$$\begin{Bmatrix} F_i^{(m,n)}(x_2) \\ I^{(m,n)}(x_2) \end{Bmatrix} = \int_A \gamma \begin{Bmatrix} \mathcal{H}_i \\ 1 \end{Bmatrix} x_1^m x_3^n\,dA \tag{9}$$

using in Eq. (6) the representation for U_i given by Eqs. (3), and performing, wherever feasible, the integration by parts, one obtains the equations of motion and the associated boundary conditions expressed solely in terms of one-dimensional quantities.

The equations of motion are

$$\delta u_2: I^{(0,0)}\ddot{u}_2 + I^{(0,1)}\ddot{\tilde{\psi}}_2 + \delta_1 I^{(1,1)}\ddot{\tilde{\tilde{\psi}}}_2 - T_{22,2}^{(0,0)} - F_2^{(0,0)} = 0 \tag{10a}$$

$$\delta\tilde{\psi}_2: I^{(0,1)}\ddot{u}_2 + I^{(0,2)}\ddot{\tilde{\psi}}_2 + \delta_1 I^{(1,2)}\ddot{\tilde{\tilde{\psi}}}_2 - T_{22,2}^{(0,1)} + T_{23}^{(0,0)} - F_2^{(0,1)} = 0 \tag{10b}$$

$$\delta\tilde{\tilde{\psi}}_{22}: I^{(1,1)}\ddot{u}_2 + I^{(1,2)}\ddot{\tilde{\psi}}_2 + \delta_1 I^{(2,2)}\ddot{\tilde{\tilde{\psi}}}_2 - \delta_1 T_{22,2}^{(1,1)} + T_{12}^{(0,1)} + T_{23}^{(1,0)} - F_2^{(1,1)} = 0 \tag{10c}$$

$$\delta h: I^{(0,0)}\ddot{h} - \left[I^{(1,0)} - x_o I^{(0,0)}\right]\ddot{\theta} - T_{23,2}^{(0,0)} - F_3^{(0,0)} - \mathcal{L} = 0 \quad (10d)$$

$$\delta\theta: \left[I^{(0,2)} + I^{(2,0)} - 2x_o I^{(1,0)} + x_o^2 I^{(0,0)}\right]\ddot{\theta} - \left[I^{(1,0)} - x_o I^{(0,0)}\right]\ddot{h} - T_{12,2}^{(0,1)} + T_{23,2}^{(1,0)} - x_o T_{23,2}^{(0,0)} - F_1^{(0,1)} + F_3^{(1,0)} - x_o F_3^{(0,0)} - \mathcal{T} = 0 \quad (10e)$$

where the expressions of mass terms $I^{(m,n)}$ are displayed in Appendix A. For a cantilevered wing, the boundary conditions (BCs) are entirely geometric at its root but entirely static at its tip. Consequently, at the root ($x_2 = 0$), these are

$$u_2 = \underline{u}_2 \quad (11a)$$

$$\tilde{\psi}_2 = \underline{\tilde{\psi}}_2 \quad (11b)$$

$$\delta_1\tilde{\tilde{\psi}}_2 = \delta_1\underline{\tilde{\tilde{\psi}}}_2 \quad (11c)$$

$$h = \underline{h} \quad (11d)$$

$$\theta = \underline{\theta} \quad (11e)$$

and at the tip ($x_2 = l$)

$$\delta u_2: T_{22}^{(0,0)} = \underline{T}_{22}^{(0,0)} \quad (12a)$$

$$\delta\tilde{\psi}_2: T_{22}^{(0,1)} = \underline{T}_{22}^{(0,1)} \quad (12b)$$

$$\delta\tilde{\tilde{\psi}}_2: \delta_1 T_{22}^{(1,1)} = \delta_1\underline{T}_{22}^{(1,1)} \quad (12c)$$

$$\delta h: T_{23}^{(0,0)} = \underline{T}_{23}^{(0,0)} \quad (12d)$$

$$\delta\theta: T_{12}^{(0,1)} - T_{23}^{(1,0)} = \underline{T}_{12}^{(0,1)} - \underline{T}_{23}^{(1,0)} \quad (12e)$$

In Eqs. (10), $\mathcal{L}$ and $\mathcal{T}$ are defined as

$$\mathcal{L}(x_2) = \int_c \Delta p\, dx_1, \qquad \mathcal{T}(x_2) = -\int_c \Delta p(x_1 - x_0)\, dx_1 \quad (13)$$

where $\Delta p = p^+ - p^-$ denotes the net transverse aerodynamic pressure acting on the external surface of the wing, and $\int_c(\cdot)\, dx_1$ is the integral in the chordwise direction.

Governing Equations

The equations of motion previously displayed are in terms of the generalized stress couples, body forces, and mass terms. To obtain the governing equations expressed in terms of the one-dimensional displacement quantities, u_2, $\tilde{\psi}_2$, $\tilde{\tilde{\psi}}_2$, h, and θ, the constitutive equations must be used.

For the sake of generality, the case of a material exhibiting elastic symmetry with respect to the plane $x_3 = 0$ (monoclinic symmetry) is considered. For this case, the three-dimensional constitutive equations in each constituent layer can be expressed as

$$\begin{Bmatrix}\sigma_{11}\\ \sigma_{22}\\ \sigma_{12}\end{Bmatrix}_{(k)} = \begin{bmatrix}\bar{Q}_{11} & \bar{Q}_{12} & \bar{Q}_{16}\\ \bar{Q}_{21} & \bar{Q}_{22} & \bar{Q}_{26}\\ \bar{Q}_{61} & \bar{Q}_{62} & \bar{Q}_{66}\end{bmatrix}_{(k)} \begin{Bmatrix}e_{11}\\ e_{22}\\ \gamma_{12}\end{Bmatrix}_{(k)} \quad (14)$$

and

$$\begin{Bmatrix}\sigma_{13}\\ \sigma_{23}\end{Bmatrix}_{(k)} = K^2 \begin{bmatrix}Q_{44} & Q_{45}\\ Q_{54} & Q_{55}\end{bmatrix}_{(k)} \begin{Bmatrix}\gamma_{13}\\ \gamma_{23}\end{Bmatrix}_{(k)} \quad (15)$$

where K^2 is the transverse shear correction factor; $Q_{ij}^{(k)}$ and $\bar{Q}_{ij}^{(k)}$ are the elastic moduli and their reduced counterparts associated with the kth layer, respectively.

Using Eqs. (4) and (8), successive integration of Eqs. (14) and (15) with respect to x_3 and x_1 yields the following one-dimensional constitutive relations for the generalized stress resultants:

$$T_{22}^{(0,0)} = \bar{A}_{22}u_{2,2} + \bar{B}_{22}\tilde{\psi}_{2,2} + \delta_1\bar{\bar{B}}_{22}\tilde{\tilde{\psi}}_{2,2} + \bar{B}_{26}\theta_{,2} + \bar{B}_{26}\tilde{\tilde{\psi}}_2 \quad (16a)$$

$$T_{22}^{(0,1)} = \bar{B}_{22}u_{2,2} + \bar{D}_{22}\tilde{\psi}_{2,2} + \delta_1\bar{\bar{D}}_{22}\tilde{\tilde{\psi}}_{2,2} + \bar{D}_{26}\theta_{,2} + \bar{D}_{26}\tilde{\tilde{\psi}}_2 \quad (16b)$$

$$T_{23}^{(0,0)} = \bar{A}_{55}\tilde{\psi}_2 + \bar{\bar{A}}_{55}\tilde{\tilde{\psi}}_2 + \bar{A}_{55}h_{,2} + \bar{A}_{55}(x_o\theta)_{,2} - \bar{\bar{A}}_{55}\theta_{,2} \quad (16c)$$

$$T_{22}^{(1,1)} = \bar{\bar{B}}_{22}u_{2,2} + \bar{\bar{D}}_{22}\tilde{\psi}_{2,2} + \delta_1\bar{\bar{\bar{D}}}_{22}\tilde{\tilde{\psi}}_{2,2} + \bar{\bar{D}}_{26}\theta_{,2} + \bar{\bar{D}}_{26}\tilde{\tilde{\psi}}_2 \quad (16d)$$

$$T_{12}^{(0,1)} = \bar{B}_{62}u_{2,2} + \bar{D}_{62}\tilde{\psi}_{2,2} + \delta_1\bar{\bar{D}}_{62}\tilde{\tilde{\psi}}_{2,2} + \bar{D}_{66}\theta_{,2} + \bar{D}_{66}\tilde{\tilde{\psi}}_2 \quad (16e)$$

$$T_{23}^{(1,0)} = \bar{A}_{55}\tilde{\psi}_2 + \bar{\bar{A}}_{55}\tilde{\tilde{\psi}}_2 + \bar{A}_{55}h_{,2} + \bar{A}_{55}(x_o\theta)_{,2} - \bar{\bar{A}}_{55}\theta_{,2} \quad (16f)$$

The expressions of stiffness quantities appearing in Eqs. (16) are displayed in Appendix A.

Substitution of Eqs. (16) into Eqs. (10) results in the following governing system:

$$\delta u_2: I^{(0,0)}\ddot{u}_2 + I^{(0,1)}\ddot{\tilde{\psi}}_2 + \delta_1 I^{(1,1)}\ddot{\tilde{\tilde{\psi}}}_2 - (\bar{A}_{22}u_{2,2} + \bar{B}_{22}\tilde{\psi}_{2,2} + \delta_1\bar{\bar{B}}_{22}\tilde{\tilde{\psi}}_{2,2} + \bar{B}_{26}\theta_{,2} + \bar{B}_{26}\tilde{\tilde{\psi}}_2)_{,2} - F_2^{(0,0)} = 0 \quad (17a)$$

$$\delta\tilde{\psi}_2: I^{(0,2)}\ddot{\tilde{\psi}}_2 + I^{(0,1)}\ddot{u}_2 + \delta_1 I^{(1,2)}\ddot{\tilde{\tilde{\psi}}}_2 - (\bar{B}_{22}u_{2,2} + \bar{D}_{22}\tilde{\psi}_{2,2} + \delta_1\bar{\bar{D}}_{22}\tilde{\tilde{\psi}}_{2,2} + \bar{D}_{26}\theta_{,2} + \bar{D}_{26}\tilde{\tilde{\psi}}_2)_{,2} + [\bar{A}_{55}\tilde{\psi}_2 + \bar{\bar{A}}_{55}\tilde{\tilde{\psi}}_2 + \bar{A}_{55}h_{,2} + \bar{A}_{55}(x_o\theta)_{,2} - \bar{\bar{A}}_{55}\theta_{,2}] - F_2^{(0,1)} = 0 \quad (17b)$$

$$\delta\tilde{\tilde{\psi}}_2: \delta_1 I^{(2,2)}\ddot{\tilde{\tilde{\psi}}}_2 + I^{(1,1)}\ddot{u}_2 + I^{(1,2)}\ddot{\tilde{\psi}}_2 - (\bar{\bar{B}}_{22}u_{2,2} + \bar{\bar{D}}_{22}\tilde{\psi}_{2,2} + \delta_1\bar{\bar{\bar{D}}}_{22}\tilde{\tilde{\psi}}_{2,2} + \bar{\bar{D}}_{26}\theta_{,2} + \bar{\bar{D}}_{26}\tilde{\tilde{\psi}}_2)_{,2} + [\bar{\bar{A}}_{55}\tilde{\psi}_2 + \bar{\bar{\bar{A}}}_{55}\tilde{\tilde{\psi}}_2 + \bar{\bar{A}}_{55}h_{,2} + \bar{\bar{A}}_{55}(x_o\theta)_{,2} - \bar{\bar{\bar{A}}}_{55}\theta_{,2}] + (\bar{B}_{62}u_{2,2} + \bar{D}_{62}\tilde{\psi}_{2,2} + \delta_1\bar{\bar{D}}_{62}\tilde{\tilde{\psi}}_{2,2} + \bar{D}_{66}\theta_{,2} + \bar{D}_{66}\tilde{\tilde{\psi}}_2) - F_2^{(1,1)} = 0 \quad (17c)$$

$$\delta h: I^{(0,0)}\ddot{h} - \left[I^{(1,0)} - x_o I^{(0,0)}\right]\ddot{\theta} - [\bar{A}_{55}\tilde{\psi}_2 + \bar{\bar{A}}_{55}\tilde{\tilde{\psi}}_2 + \bar{A}_{55}h_{,2} + \bar{A}_{55}(x_o\theta)_{,2} - \bar{\bar{A}}_{55}\theta_{,2}]_{,2} - F_3^{(0,0)} - \mathcal{L} = 0 \quad (17d)$$

$$\delta\theta: \left[I^{(0,2)} + I^{(2,0)} - 2x_o I^{(1,0)} + x_o^2 I^{(0,0)}\right]\ddot{\theta} - \left[I^{(1,0)} - x_o I^{(0,0)}\right]\ddot{h} - (\bar{B}_{62}u_{2,2} + \bar{D}_{62}\tilde{\psi}_{2,2} + \delta_1\bar{\bar{D}}_{62}\tilde{\tilde{\psi}}_{2,2} + \bar{D}_{66}\theta_{,2} + \bar{D}_{66}\tilde{\tilde{\psi}}_2)_{,2} + [\bar{\bar{A}}_{55}\tilde{\psi}_2 + \bar{\bar{\bar{A}}}_{55}\tilde{\tilde{\psi}}_2 + \bar{\bar{A}}_{55}h_{,2} + \bar{\bar{A}}_{55}(x_o\theta)_{,2} - \bar{\bar{\bar{A}}}_{55}\theta_{,2}]_{,2} - x_o[\bar{A}_{55}\tilde{\psi}_2 + \bar{\bar{A}}_{55}\tilde{\tilde{\psi}}_2 + \bar{A}_{55}h_{,2} + \bar{A}_{55}(x_o\theta)_{,2} - \bar{\bar{A}}_{55}\theta_{,2}]_{,2} - F_1^{(0,1)} + F_3^{(1,0)} - x_o F_3^{(0,0)} - \mathcal{T} = 0 \quad (17e)$$

A procedure similar to that used to obtain the above equations can be applied to convert the static boundary conditions (at the wing tip) in terms of the displacement quantities.

System (17) is tenth order in terms of the basic unknown functions u_2, $\tilde{\psi}_2$, $\tilde{\tilde{\psi}}_2$, h, and θ. However, as shown in Ref. 13, by removing the in-plane body forces and rotatory inertia terms, which are negligibly small, the governing equations can be reduced to a system of four equations in terms of $\tilde{\psi}_2$, $\tilde{\tilde{\psi}}_2$, θ, and h, only.

Moreover, the BCs also can be reduced to four conditions at $x_2 = 0, l$. This reduction can be done by eliminating u_2 from system (17) with the help of

$$u_{2,2} = -(1/\bar{A}_{22})(\bar{B}_{22}\tilde{\psi}_{2,2} + \delta_1\bar{\bar{B}}_{22}\tilde{\tilde{\psi}}_{2,2} + \bar{B}_{26}\theta_{,2} + \bar{B}_{26}\tilde{\tilde{\psi}}_2) \quad (18)$$

The BCs to be prescribed at $x_2 = 0$ are $\tilde{\psi}_2 = \underline{\tilde{\psi}}_2$, $\delta_1\tilde{\tilde{\psi}}_2 = \delta_1\underline{\tilde{\tilde{\psi}}}_2$; $h = \underline{h}$, and $\theta = \underline{\theta}$. The BCs at $x_2 = l$ are not displayed here. In this case, the resulting eighth-order system is consistent with the number of four boundary conditions to be prescribed at each edge.

Under this form, the aeroelastic governing equations include the effects of anisotropy and heterogeneity, transverse shear, and WR. In

addition, the thickness of the wing $H\{\equiv \sum_{k=1}^{N}[z_{(k)}-z_{(k-1)}]\}$ could exhibit a variability in both the chordwise and spanwise directions. In this case, the governing equations feature variable coefficients in the x_2 direction. This complexity is not considered further in this paper.

Flutter of Uniform Swept Wings Featuring Transverse-Shear and WR Effects

The previously displayed equations incorporate a number of nonclassical effects that dramatically influence flutter and divergence instability of aircraft wings.

Among these, the anisotropy and heterogeneity can be used to enhance the aeroelastic behavior in both subcritical and critical ranges. This procedure, referred to as aeroelastic tailoring, has been developed in a number of theoretical studies[2,4,10–13] and applied successfully in the aeronautics industry, perhaps one of the most spectacular products being the experimental forward-swept-wing aircraft Grumman X-29.

However, aeroelastic tailoring is not addressed in the present work. Instead, two effects whose implications in flutter instability have not yet been studied are considered. These effects are the WR and transverse shear flexibility. Toward the goal of a comprehensive assessment of their influence, the problem is simplified without sacrificing generality. The wing is assumed to be symmetrically composed of transversely isotropic material layers featuring uniform (geometric and physical) properties in the spanwise direction. It is further stipulated that the reference axis coincides with the wing midchord.

Under such conditions, a number of stiffness quantities vanish, i.e., $\bar{\bar{A}}_{ij} = \bar{\bar{D}}_{ij} \equiv 0$ and $\bar{B}_{ij} = \bar{\bar{B}}_{ij} = \bar{\bar{\bar{B}}}_{ij} \equiv 0$. As a result, the aeroelastic governing system of equations becomes

$$\bar{D}_{22}\tilde{\psi}_{2,22} - \bar{A}_{55}\tilde{\psi}_2 - \bar{A}_{55}h_{,2} - x_o\bar{A}_{55}\theta_{,2} = 0 \tag{19a}$$

$$(\bar{D}_{66} + \bar{\bar{\bar{A}}}_{55})\tilde{\bar{\psi}}_2 + (\bar{D}_{66} - \bar{\bar{\bar{A}}}_{55})\theta_{,2} - \delta_1\bar{\bar{\bar{D}}}_{22}\tilde{\bar{\psi}}_{2,22} = 0 \tag{19b}$$

$$I^{(0,0)}\ddot{h} - \left[I^{(1,0)} - x_o I^{(0,0)}\right]\ddot{\theta} - \bar{A}_{55}\tilde{\psi}_{2,2} - \bar{A}_{55}h_{,22} - \bar{A}_{55}x_o\theta_{,22} - \mathcal{L} = 0 \tag{19c}$$

$$\left[I^{(0,2)} + I^{(2,0)} - 2x_o I^{(1,0)} + x_o^2 I^{(0,0)}\right]\ddot{\theta} - \left[I^{(1,0)} - x_o I^{(0,0)}\right]\ddot{h} - (\bar{D}_{66} + \bar{\bar{\bar{A}}}_{55})\theta_{,22} - (\bar{D}_{66} - \bar{\bar{\bar{A}}}_{55})\tilde{\bar{\psi}}_{,2} - x_o(\bar{A}_{55}\tilde{\psi}_{2,2} + \bar{A}_{55}h_{,22} + x_o\bar{A}_{55}\theta_{,22}) - \mathcal{T} = 0 \tag{19d}$$

and the associated homogeneous boundary conditions are

$$\text{At } x_2 = 0: \qquad \tilde{\psi}_2 = \tilde{\bar{\psi}}_2 = h = \theta = 0 \tag{20}$$

$$\text{At } x_2 = l: \qquad \tilde{\psi}_{2,2} = 0 \tag{21a}$$

$$\tilde{\bar{\psi}}_{2,2} = 0 \tag{21b}$$

$$\tilde{\psi}_2 + h_{,2} + x_o\theta_{,2} = 0 \tag{21c}$$

$$(\bar{D}_{66} - \bar{\bar{\bar{A}}}_5)\tilde{\bar{\psi}}_2 + (\bar{D}_{66} + \bar{\bar{\bar{A}}}_{55})\theta_{,2} = 0 \tag{21d}$$

For such a type of anisotropy, the nonzero elastic coefficients intervening in Eqs. (A1d and A1e) are[20]

$$\bar{Q}_{11} = \bar{Q}_{22} = \frac{E}{1-\nu^2}; \qquad \bar{Q}_{12} = \frac{E\nu}{1-\nu^2}$$
$$\bar{Q}_{66} = G_{12}\left[\equiv \frac{E}{2(1+\nu)}\right]; \qquad Q_{44} = Q_{55} = G' \tag{22}$$

Because of their outstanding thermomechanical properties, materials featuring this type of anisotropy are likely to play a major role in the construction of the supersonic and hypersonic flight vehicles.[21,22] For such a case, the explicit relation for the stiffness quantities appearing in Eqs. (19) are obtained by substituting Eqs. (22) into Eqs. (A1d and A1e) through the use of Eqs. (A1a–A1c).

For flutter analysis, harmonic time dependence is assumed for both the unsteady loads and the displacement quantities, $\tilde{\psi}_2$, $\tilde{\bar{\psi}}_2$, h, and θ. This implies that, for a generic quantity $\mathcal{F}$ (which can imply each of $\tilde{\psi}_2$, $\tilde{\bar{\psi}}_2$, h, θ, $\mathcal{L}$, and $\mathcal{T}$), the representation $\mathcal{F}(x_2;t) = \mathrm{Re}[\hat{\mathcal{F}}(x_2)\exp(i\omega t)]$ is used, where $\hat{\mathcal{F}}$ denotes the complex amplitude of $\mathcal{F}$ and Re $(\cdot)$ denotes the real part of $(\cdot)$.

The harmonic amplitudes $\hat{\mathcal{L}}$ and $\hat{\mathcal{T}}$ corresponding to a swept wing whose cross sections are normal to the elastic axis are[18]

$$\hat{\mathcal{L}}(\eta) = \tfrac{1}{8}\pi\rho\omega^2c^3\left(L_{hh}\hat{h}_* + L_{h\theta}\hat{\theta}_* + L_{hh'}\hat{h}'_* + L_{h\theta'}\hat{\theta}'_*\right) \tag{23a}$$

$$\hat{\mathcal{T}}(\eta) = \tfrac{1}{16}\pi\rho\omega^2c^4\left(M_{\theta h}\hat{h}_* + M_{\theta\theta}\hat{\theta}_* + M_{\theta h'}\hat{h}'_* + M_{\theta\theta'}\hat{\theta}'_*\right) \tag{23b}$$

where $\hat{h}_* = \hat{h}/c$ and $\hat{\theta}_* \equiv \hat{\theta}$ are dimensionless quantities associated with the plunging and twist amplitude, respectively; ρ the gas density; and $()' \equiv \partial()/\partial\eta$.

In Eqs. (23), L_{hh}, $L_{h\theta}$, $L_{hh'}$, …, $M_{\theta\theta'}$ represent the dimensionless aerodynamic coefficients whose expressions are displayed in Appendix B. In these coefficients, V_n is the speed component normal to the leading edge.

For the case of the wing composed of a single transversely isotropic material layer, the aeroelastic governing equations can be cast in the form of two coupled ordinary differential equations in terms of $\hat{h}_*$ and $\hat{\theta}_*$ as

$$\hat{h}_*'''' + c_1\hat{h}_*''' + c_3\hat{h}_*'' + d_1\hat{h}_*' + d_3\hat{h}_* + \tfrac{1}{2}a\hat{\theta}_*'''' + c_2\hat{\theta}_*''' + c_4\hat{\theta}_*'' + d_2\hat{\theta}_*' + d_4\hat{\theta}_* = 0 \tag{24a}$$

$$(\delta_1/12)(1+E_2)\hat{\theta}_*'''' + \delta_1E_1c_{11}\hat{\theta}_*''' + (\delta_1E_1c_{12} - c_{13})\hat{\theta}_*'' - (1+E_2)c_{11}\hat{\theta}_*' - (1+E_2)c_{12}\hat{\theta}_* + \delta_1E_1c_{14}\hat{h}_*''' + \delta_1E_1c_{15}\hat{h}_*'' - (1+E_2)c_{14}\hat{h}_*' - (1+E_2)c_{15}\hat{h}_* = 0 \tag{24b}$$

Consistent with the eighth order of the governing equations, four boundary conditions must be prescribed at each edge, namely,

$$\text{At } \eta = 0: \qquad \hat{h}_* = \hat{\theta}_* = 0 \tag{25a,b}$$

$$E_1\hat{h}_*''' + E_1c_1\hat{h}_*'' + (1+E_1c_3)\hat{h}_*' + \tfrac{1}{2}aE_1\hat{\theta}_*''' + E_1c_2\hat{\theta}_*'' + \left(\tfrac{1}{2}a + E_1c_4\right)\hat{\theta}_*' = 0 \tag{25c}$$

$$\delta_1E_1\left[\frac{1+E_2}{12}\hat{\theta}_*''' + E_1c_{11}\hat{\theta}_*'' + E_1c_{12}\hat{\theta}_*' + E_1c_{14}\hat{h}_*'' + E_1c_{15}\hat{h}_*'\right] + \frac{(1-E_2)^2}{12}\hat{\theta}_*' = 0 \tag{25d}$$

and

$$\text{at } \eta = 1: \quad \hat{h}_*'' + c_1\hat{h}_*' + c_3\hat{h}_* + \tfrac{1}{2}a\hat{\theta}_*'' + c_2\hat{\theta}_*' + c_4\hat{\theta}_* = 0 \tag{26a}$$

$$[(1+E_2)/12]\hat{\theta}_*'' + E_1c_{11}\hat{\theta}_*' + E_1c_{12}\hat{\theta}_* + E_1c_{14}\hat{h}_*' + E_1c_{15}\hat{h}_* = 0 \tag{26b}$$

$$\hat{h}_*''' + c_1\hat{h}_*'' + c_3\hat{h}_*' + \tfrac{1}{2}a\hat{\theta}_*''' + c_2\hat{\theta}_*'' + c_4\hat{\theta}_*' = 0 \tag{26c}$$

$$\delta_1\left\{[(1+E_2)/12]\hat{\theta}_*''' + E_1c_{11}\hat{\theta}_*'' + E_1c_{12}\hat{\theta}_*' + E_1c_{14}\hat{h}_*'' + E_1c_{15}\hat{h}_*'\right\} - c_{13}\hat{\theta}_*' = 0 \tag{26d}$$

The nondimensional coefficients appearing in the preceding equations are functions of inertia and structural and aerodynamic parameters and are displayed in Appendix C.

Flutter Solution Methodology

The eigenvalue problem described by Eqs. (24) in conjunction with the BCs in Eqs. (25) and (26) can be solved exactly via the Laplace transform method applied in the space domain. Defining

$$\mathcal{H}(s) \equiv LT[\hat{h}_*(\eta)], \qquad \Theta(s) \equiv LT[\hat{\theta}_*(\eta)] \tag{27}$$

as the Laplace transforms of $\hat{h}_*(\eta)$ and $\hat{\theta}_*(\eta)$, respectively, the ordinary differential equations (24) can be reduced to a set of two algebraic equations in $\mathcal{H}$ and Θ whose coefficients are polynomials in the complex variable s.

In this form, the equations can be written formally as

$$\begin{bmatrix} \mathcal{A}(s) & \mathcal{B}(s) \\ \mathcal{C}(s) & \mathcal{D}(s) \end{bmatrix} \begin{Bmatrix} \mathcal{H} \\ \Theta \end{Bmatrix} = \begin{Bmatrix} b_1 \\ b_2 \end{Bmatrix} \tag{28}$$

where $\mathcal{A}$, $\mathcal{B}$, $\mathcal{C}$, and $\mathcal{D}$ are polynomials in s whose coefficients include all the geometric, structural, and aerodynamic properties of the wing.

In the process of applying the Laplace transformation to Eqs. (24), the four boundary conditions in Eqs. (25) at $\eta = 0$ are used. The additional unknown quantities $\hat{h}'_*(0)$, $\hat{h}''_*(0)$, $\hat{\theta}'_*(0)$, and $\hat{\theta}''_*(0)$ (referred to as residual terms) appear when carrying out the Laplace transform. Solving the linear system (28) and taking the inverse Laplace transforms of $\mathcal{H}$, and Θ, the mode shapes $\hat{h}_*(\eta)$ and $\hat{\theta}_*(\eta)$ can be expressed formally as

$$\hat{h}_*(\eta) = H_{10}(\eta)\hat{h}'_*(0) + H_{20}(\eta)\hat{h}''_*(0) + H_{30}(\eta)\hat{\theta}'_*(0) + H_{40}(\eta)\hat{\theta}''_*(0) \tag{29a}$$

$$\hat{\theta}_*(\eta) = T_{10}(\eta)\hat{h}'_*(0) + T_{20}(\eta)\hat{h}''_*(0) + T_{30}(\eta)\hat{\theta}'_*(0) + T_{40}(\eta)\hat{\theta}''_*(0) \tag{29b}$$

where $H_{io}(\eta)$ and $T_{io}(\eta)$, $(i = \overline{1,4})$ are known functions (not displayed here).

Fulfillment of the remaining four boundary conditions in Eqs. (26) at $\eta = 1$ yields an algebraic system of homogeneous equations for the residual terms expressed as

$$DY = 0 \tag{30}$$

where $Y \equiv [\hat{h}'_*(0), \hat{h}''_*(0), \hat{\theta}'_*(0), \hat{\theta}''_*(0)]^T$ and $[D]$ is a 4×4 matrix whose elements are complex valued and include all the geometric, aerodynamic, and material properties of the wing. Moreover, k and ω (which, for neutral stability conditions, should be real valued quantities), appear explicitly.

The flutter is determined from the condition of nontrivial solution of the homogeneous system (30), by requiring its determinant $[D]$ (referred to as the flutter determinant) to vanish.

In contrast to the case where the modal methods are employed, for which the flutter determinant has the same order as the preselected number of generalized modes, in the present case its order is one-half that of the original system of ordinary differential equations.

For given geometry, flight conditions, and material properties, the values of $1/k$ and X causing both the real and the imaginary parts of $[D]$ to vanish simultaneously yield the flutter speed and flutter frequency. The procedure applied to determine these critical values involves a trial-and-error process.[19] The normalized flutter-mode shapes $\hat{h}_*(\eta)/\hat{h}'_*(0)$ and $\hat{\theta}_*(\eta)/\hat{h}'_*(0)$ can then be determined from Eqs. (29) by solving the reduced system (30) in terms of the three normalized modes $\hat{h}''_*(0)/\hat{h}'_*(0)$, $\hat{\theta}'_*(0)/\hat{h}'_*(0)$, and $\hat{\theta}''_*(0)/\hat{h}'_*(0)$.

A slightly modified version of this technique also can be applied to analyze the aeroelastic static response in both subcritical and critical flight regimes of laminated composite swept wings. Since the divergence instability boundary occurs at $\omega = 0$, the elements of the matrix $[D]$ have to be correspondingly modified to obtain from $[\hat{D}] = 0$ the critical dynamic pressure, i.e., $(Q_n)_{\text{div}}$, where $[\hat{D}]$ is the modified static counterpart of $[D]$, which, for this problem, is purely real.

For the study of the subcritical static aeroelastic response, the governing equations reduce to $\hat{D}Y = B$, where B is a 4×1 column vector whose elements have been defined in Ref. 13. In such a case, determination of the vector Y, which, in conjunction with Eqs. (29), yields all the elements pertinent to the subcritical static aeroelastic response, is required.

Numerical Results

Before proceeding to the numerical validation of the solution methodology and assessment of the nonclassical effects, several remarks are in order.

One of them is related to the transverse shear flexibility measured in terms of the ratio E/G'. In advanced composite materials, the transverse shear flexibility parameter R can take values of 100 or larger. For the classical case, owing to the infinite transverse shear stiffness featured by the metallic material structures, $E/G' \to 0$.

Concerning the warping inhibition, the system of equations and the associated boundary conditions incorporating this effect are obtained by taking $\delta_1 = 1$ in Eqs. (24–26); for the FW case, $\delta_1 = 0$. In the former case, the governing equation system is eighth order (requiring fulfillment of four BCs at each end of the wing); the latter case is sixth order, and consequently, only three BCs must be prescribed at each end.

To verify the accuracy of the flutter analysis, a number of comparisons for a test case were carried out. The comparisons concern the flutter predictions of a cantilever rectangular straight metallic wing of $AR = 6.67$ as given in Ref. 23 (with a subsequent appended correction of the flutter results in Ref. 24).

The results reveal that the predictions provided by the present approach, i.e., $V_F = 495$ km/h and $\omega_F = 11.20$ Hz are in excellent agreement with Goland's exact results, namely $V_F = 494$ km/h and $\omega_F = 11.25$ Hz. At the same time, compared with the predictions obtained via a number of computer codes[9,25] or other solution methodologies,[26] one can conclude that the methodology used in this paper constitutes a highly accurate, powerful, and versatile tool for a cost-effective aeroelastic parametric study.

For Goland's wing (GW, for a wing featuring geometric parameters similar to those in Ref. 23), Figs. 2 and 3 display the variation of the flutter speed parameter λ_F and of the flutter frequency parameter Ω_F vs the tranverse shear parameter R for the case of an unswept wing and for the FW and WR models. Here, the reference frequency ω_R is taken to be the natural bending frequency, ω_h.

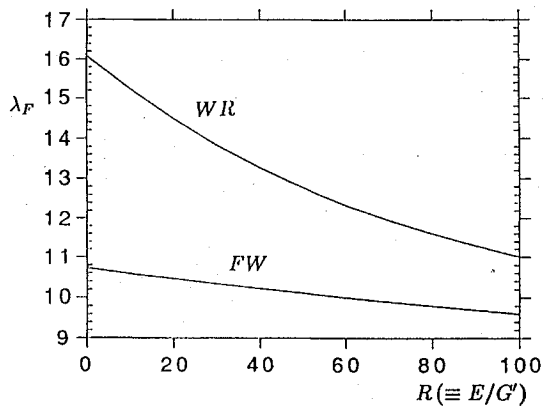

Fig. 2 Flutter speed λ_F vs transverse shear flexibility parameter for an unswept wing of $AR = 6.67$ (GW) and for FW and WR models.

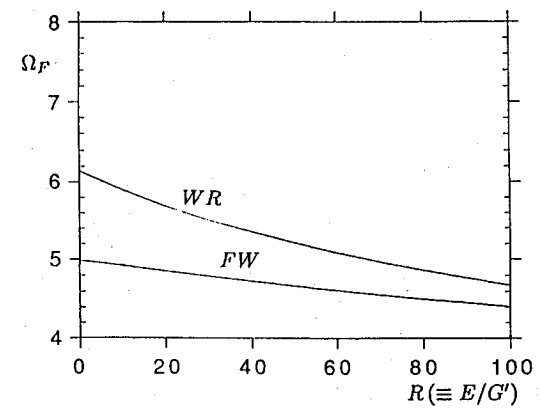

Fig. 3 Flutter frequency Ω_F vs transverse shear flexibility parameter for an unswept wing of $AR = 6.67$ (GW) and for FW and WR models.

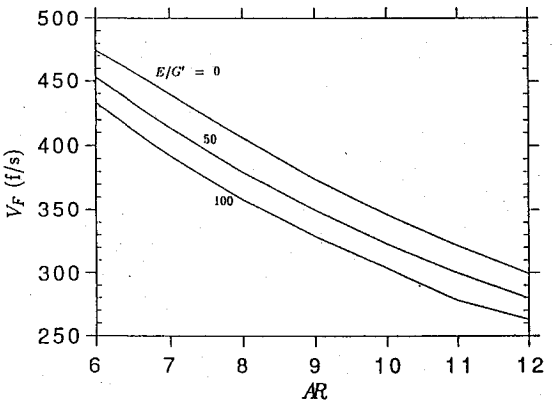

Fig. 4 Effect of aspect ratio on flutter speed of an unswept wing (GW) for three values of the transverse shear flexibility parameter.

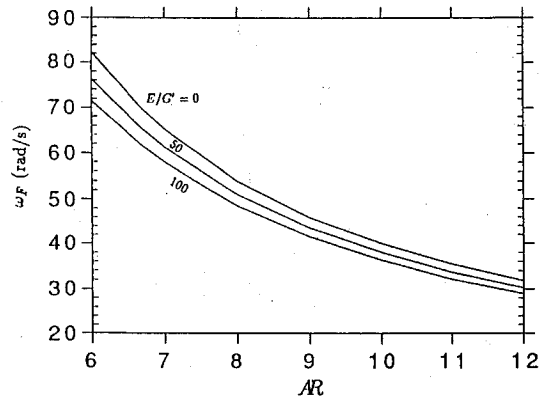

Fig. 5 Effect of aspect ratio on flutter frequency of an unswept wing (GW) for three values of the transverse shear flexibility parameter.

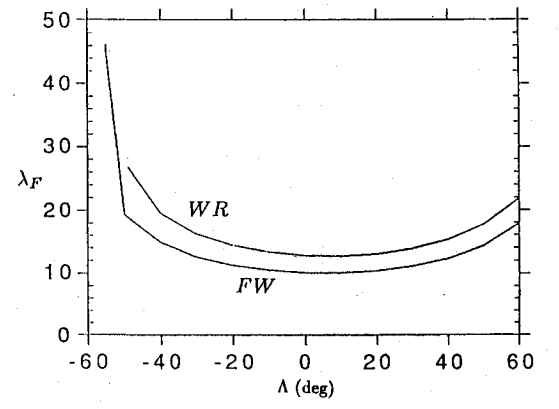

Fig. 6 Effect of sweep angle on flutter speed parameter of the GW for WR and FW models.

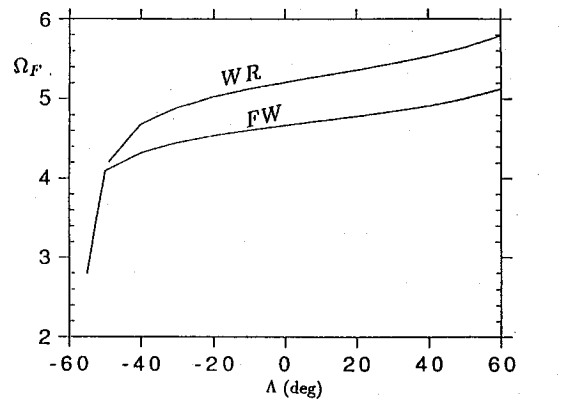

Fig. 7 Effect of sweep angle on flutter frequency parameter of the GW for WR and FW models.

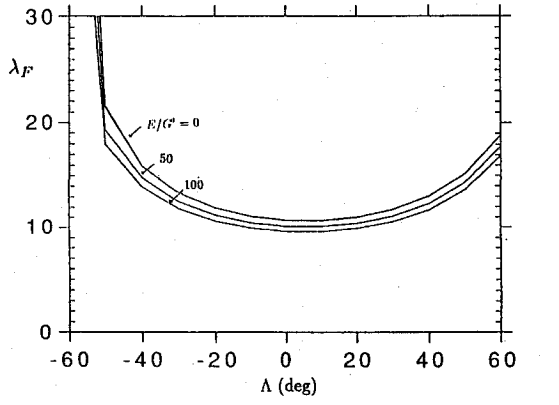

Fig. 8 Effect of sweep angle on flutter speed parameter for classical ($R = 0$) and shear deformable wings.

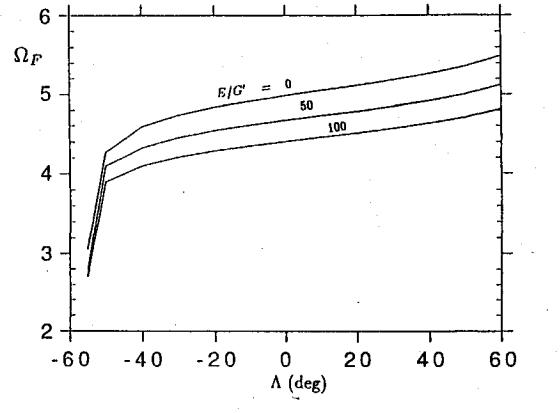

Fig. 9 Effect of sweep angle on flutter frequency parameter of classical ($R = 0$) and shear deformable wings.

As in the case of the panel flutter,[20] the results reveal that, with the increase of transverse shear flexibility, the flutter becomes more critical. The same graphs show that the WR results in an increase of the flutter speed and flutter frequency compared with the FW wing counterpart. However, with the increase of the parameter R, the decay of the flutter speed and frequency is more dramatic in the case of the wing structures featuring the WR than in the FW case. A similar trend was obtained in the context of the dynamic response under time-dependent excitation of a cantilever wing modeled as a thin-walled beam.[27] Herein, ω_h is held fixed in all calculations ($\omega_h = 14.0613$ rad/s). For the same unswept wing, Figs. 4 and 5 depict the variations of the flutter speed V_F and flutter frequency ω_F vs wing aspect ratio for three values of the R parameter. In all of these results, the FW wing model was adopted and the chord length was held constant ($c = 6$ ft).

These graphs show that the increase in both the aspect ratio and the transverse shear flexibility results in a decrease of the flutter speed and frequency. Moreover, Fig. 5 shows that, for large-aspect-ratio wings, ω_F is less sensitive to the increase of the transverse shear flexibility. Two sets of results (Figs. 6 and 7, Figs. 8 and 9) emphasizing the influence of the wing sweep angle are presented.

In Figs. 6 and 7, the variations of the flutter speed and frequency parameters λ_F and Ω_F vs the sweep angle Λ, respectively, for the cases of FW and WR are displayed. These results are obtained for a constant transverse shear flexibility parameter $R = 50$. The trend of variation of the flutter speed vs the sweep angle as depicted in Fig. 6 is similar to the one in Refs. 8 and 18. The results reveal that the flutter frequency decreases continuously with decreasing Λ, and that this decrease is at a greater rate for WR wings than for the FW counterparts.

In Figs. 8 and 9, the variations of λ_F and Ω_F vs $\Lambda (\gtrless 0)$ for three values of R and for the FW case are displayed. These plots reveal that the trend of variation appearing in Figs. 6 and 7 remains the same and that the transverse shear flexibility has a deleterious effect on both the flutter speed and the frequency.

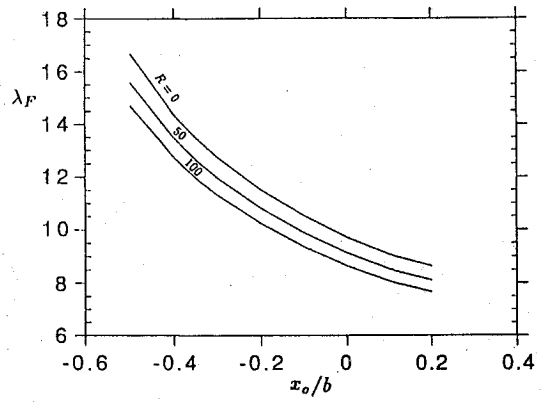

Fig. 10 Effect of pitch axis location on flutter speed parameter for classical (R = 0) and shear deformable wings (Λ = −30 deg, FW wing model).

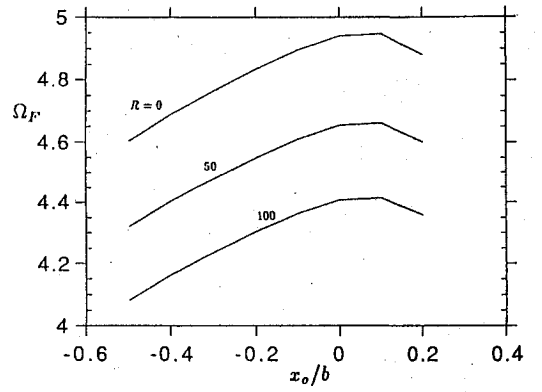

Fig. 11 Effect of pitch axis location on flutter frequency parameter for classical (R = 0) and shear deformable wings (Λ = −30 deg, FW wing model).

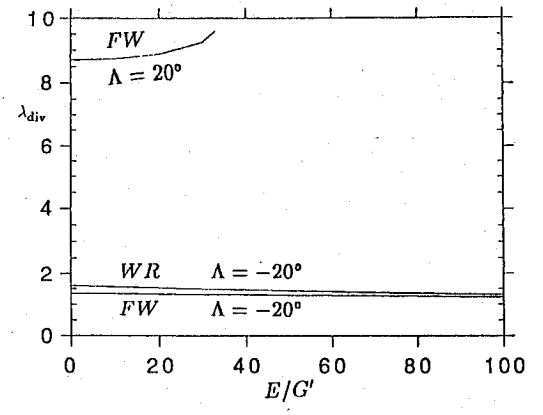

Fig. 12 Effect of transverse shear on divergence speed parameter of the back-swept or forward-swept GW for FW and WR models.

The influence of the elastic axis location measured in terms of the dimensionless parameter $\bar{x}_o(\equiv x_o/b)$, (positive when aft is the reference axis) upon λ_F and Ω_F is depicted in Figs. 10 and 11, for three values of $R(0, 50, 100)$, one value of $\Lambda(-30\,\text{deg})$, and for the FW wing model. The results show the usual trend, namely, that the flutter speed decreases as the elastic axis moves aft, increasing the distance between the elastic axis and the aerodynamic center.

Finally, Fig. 12 shows the influence of the transverse shear flexibility on the divergence speed parameter $\lambda_{\text{div}}[\equiv (Q_n)_{\text{div}}^{1/2}/\cos\Lambda]$ of a forward-swept or back-swept wing when both FW and WR are considered.

The results in this figure reveal that the transverse shear flexibility exacerbates the wash-in effect for forward-swept wings and the wash-out effect for back-swept wings. This trend is similar to the one obtained within a thin-walled wing model.[28] The numerical results also confirm the well-known fact that the divergence speed of forward-swept wings is considerably lower than that of their aft-swept-wing counterparts. Moreover, results not explicitly displayed but easily anticipated from Fig. 12 show that the wing is free of divergence instability for $\Lambda > 20$ deg.

Conclusions

A comprehensive approach to the static and dynamic aeroelastic instabilities of cantilevered wings, based on an advanced structural model, is presented. Using this model, an aeroelastic tailoring study allowing optimization of the structure from an aeroelastic perspective can be implemented. However, the main focus of the paper rests on the assessment of nonclassical effects not considered heretofore, i.e., transverse shear flexibility and WR.

The results demonstrate the great influence of the two main effects, considered individually or together, on the flutter and divergence instabilities as well as the error incurred when these effects are neglected.

To predict the aeroelastic instability phenomena as accurately as possible, these effects must always be incorporated during the earliest phases of the design and their influence assessed. In connection with the effect of the WR as considered in this work, a word of caution is in order. Because of the character of anisotropy considered herein, the bending-twist cross-coupling becomes immaterial. However, for a generalized orthotropy of the material, this elastic cross-coupling will be induced and in circumstances shown in other papers dealing with static aeroelasticity,[10–12] the WR wing model can yield more conservative predictions than its FW counterpart. A similar trend could occur in the case of the flutter instability, as well. In any case, the clarification of this issue warrants further investigation. Moreover, even in the case of a wing model infinitely rigid in transverse shear,[8,29] the bending-twist cross-coupling significantly influences the flutter boundary, an effect opposite to that exerted on the divergence instability. This further enforces the conclusion that the nonclassical effects studied within these numerical illustrations, and the other effects incorporated in the present theory, must always be considered in the aeroelastic design of advanced flight vehicles.

Finally, the Laplace transform method used to determine flutter and divergence instability boundaries[30] constitutes a powerful mathematical tool of high efficiency and robustness, even when extensive parametric studies must be performed.

Appendix A: Expressions of the One-Dimensional Stiffness Quantities

$$[\bar{A}_{ij}(x_2), \bar{\bar{A}}_{ij}(x_2), \bar{\bar{\bar{A}}}_{ij}(x_2)] = \int_c A_{ij}\left[1, x_1, x_1^2\right] dx_1 \quad \text{(A1a)}$$

$$[\bar{B}_{ij}(x_2), \bar{\bar{B}}_{ij}(x_2), \bar{\bar{\bar{B}}}_{ij}(x_2)] = \int_c B_{ij}\left[1, x_1, x_1^2\right] dx_1 \quad \text{(A1b)}$$

$$[\bar{D}_{ij}(x_2), \bar{\bar{D}}_{ij}(x_2), \bar{\bar{\bar{D}}}_{ij}(x_2)] = \int_c D_{ij}\left[1, x_1, x_1^2\right] dx_1 \quad \text{(A1c)}$$

where $c[\equiv c(x_2)]$ denotes the wing chord, and

$$[A_{ij}(x_1, x_2), B_{ij}(x_1, x_2), D_{ij}(x_1, x_2)] = \sum_{k=1}^{N} \int_{z_{(k-1)}}^{z_{(k)}} \bar{Q}_{ij}^{(k)}\left[1, x_3, x_3^2\right] dx_3 \quad \text{(A1d)}$$

$$A_{55}(x_1, x_2) = K^2 \sum_{k=1}^{N} \int_{z_{(k-1)}}^{z_{(k)}} Q_{55}^{(k)}\, dx_3 \quad \text{(A1e)}$$

where K^2 is a transverse shear correction factor.

The mass terms $I^{(m,n)}$ are defined as

$$I^{(m,n)} = \int_c x_1^m M_{n+1}\, dx_1 \quad \text{(A1f)}$$

where

$$M_n = \frac{1}{n} \sum_{k=1}^{N} \gamma_{(k)}\left(z_{(k)}^n - z_{(k-1)}^n\right) \quad \text{(A1g)}$$

where $\gamma_{(k)}$ is the mass density of the kth-layer material.

Appendix B: Nondimensional Aerodynamic Coefficients Appearing in Eqs. (23)

$$L_{hh} = 2L_h \tag{B1a}$$

$$L_{hh'} = (2/\mathcal{R})[-i(V_n/\omega b)\tan\Lambda]L_h \tag{B1b}$$

$$L_{h\theta} = L_\theta - \left(\tfrac{1}{2} + a\right)L_h \tag{B1c}$$

$$L_{h\theta'} = (2/\mathcal{R})[-i(\tan\Lambda/k)]\left[-\tfrac{1}{2} + \left(\tfrac{1}{2} - a\right)L_h\right] \tag{B1d}$$

$$M_{\theta h} = 2\left[M_h - \left(\tfrac{1}{2} + a\right)L_h\right] \tag{B1e}$$

$$M_{\theta h'} = (2/\mathcal{R})[-i(\tan\Lambda/k)]M_{\theta h} \tag{B1f}$$

$$M_{\theta\theta} = M_\theta - \left(\tfrac{1}{2} + a\right)(M_h + L_\theta) + \left(\tfrac{1}{2} + a\right)^2 L_h \tag{B1g}$$

$$M_{\theta\theta'} = (2/\mathcal{R})[-i(\tan\Lambda/k)]\left[\tfrac{3}{8} - (i/2k) - \left(\tfrac{1}{4} - a^2\right)L_h\right] \tag{B1h}$$

where

$$L_h = 1 - 2i[C(k)/k] \tag{B1i}$$

$$L_\theta = \tfrac{1}{2} - (i/k) - (2i/k)C(k) - (2/k^2)C(k) \tag{B1j}$$

$$M_\theta = \tfrac{3}{8} - (i/k) \tag{B1k}$$

$$M_h = \tfrac{1}{2} \tag{B1l}$$

Appendix C: Expression of Coefficients Appearing in Eqs. (24–26)

$$E_1\left(\equiv \frac{\bar{\bar{D}}_{22}}{\ell^2 \bar{\bar{A}}_{55}}\right) = \frac{(H^*/\mathcal{R})^2}{12(1-\nu^2)}E/G'$$

$$E_2\left(\equiv \frac{\bar{D}_{66}}{\bar{\bar{A}}_{55}}\right) = \frac{H_*^2}{8(1+\nu)}E/G'$$

$$c_1 = E_1\Omega^2(L_{hh'}/8\mu_o), \qquad c_2 = E_1\Omega^2(L_{h\theta'}/8\mu_o)$$

$$c_3 = E_1\Omega^2[1 + (L_{hh}/8\mu_o)]$$

$$c_4 = -\tfrac{1}{2}E_1\Omega^2[\bar{X}_\alpha - (L_{h\theta}/4\mu_o)]$$

$$c_5 = (a^2/4) + (1 + E_2)/12, \qquad c_6 = (E_2 - 1)/12$$

$$c_7 = E_1\Omega^2(M_{\theta h'}/16\mu_o), \qquad c_8 = E_1\Omega^2(M_{\theta\theta'}/16\mu_o)$$

$$c_9 = -\tfrac{1}{2}E_1\Omega^2[\bar{X}_\alpha - (M_{\theta h}/8\mu_o)]$$

$$c_{10} = \tfrac{1}{4}E_1\Omega^2[\bar{I}_\alpha + (M_{\theta\theta}/4\mu_o)], \qquad c_{11} = (1/E_1)\left(c_8 - \tfrac{1}{2}ac_2\right)$$

$$c_{12} = (\Omega^2/4)\{\bar{I}_\alpha + (M_{\theta\theta}/4\mu_o) + a[\bar{X}_\alpha - (L_{h\theta}/4\mu_o)]\}$$

$$c_{13} = E_2/3E_1, \qquad c_{14} = \left(\Omega^2/16\mu_o\right)(M_{\theta h'} - aL_{hh'})$$

$$c_{15} = -\frac{\Omega^2}{2}\left(a + \bar{X}_\alpha + \frac{aL_{hh} - M_{\theta h}}{8\mu_o}\right)$$

$$d_1 = -(c_1/E_1), \qquad d_2 = -(c_2/E_1)$$

$$d_3 = -(c_3/E_1), \qquad d_4 = -(c_4/E_1)$$

In these expressions, the following notations have been used:

$$\Omega = (\omega/\omega_h) \qquad \text{where} \qquad \omega_h \equiv \left(\bar{D}_{22}/ml^4\right)^{\frac{1}{2}}$$

$$\mu_o = [m/\pi\rho(2b)^2] \qquad \text{where} \qquad m = I^{(0,0)}$$

$$I_\alpha = I^{(0,2)} + I^{(2,0)} - 2x_o I^{(1,0)} + x_o^2 I^{(0,0)}$$

$$mX_\alpha = I^{(1,0)} - x_o I^{(0,0)}, \qquad \bar{X}_\alpha = X_\alpha/b, \qquad \bar{I}_\alpha = I_\alpha/mb^2$$

Acknowledgment

The authors are grateful for the support of the U.S. Naval Academy for partial funding.

References

[1]Wilson, E. G., "Static Aeroelasticity in the Design of Modern Fighters," *Static Aeroelasticity in Combat Aircraft*, AGARD Rept. 725, Jan. 1986.

[2]Weisshaar, T. A., "Aeroelastic Tailoring, Creative Uses of Unusual Materials," AIAA Paper 87-0976, 1987.

[3]Weisshaar, T. A., "Divergence of Forward Swept Composite Wings," *Journal of Aircraft*, Vol. 17, No. 6, 1980, pp. 442–448.

[4]Weisshaar, T. A., "Aeroelastic Tailoring of Forward Swept Composite Wings," *Journal of Aircraft*, Vol. 18, No. 8, 1981, pp. 669–676.

[5]Niblett, L. T., "Divergence and Flutter of Swept-Forward Wings with Cross-Flexibilities," RAE-TR-80047, April 1980.

[6]Hollowell, S. J., and Dugundji, J., "Aeroelastic Flutter and Divergence of Stiffness Coupled, Graphite/Epoxy, Cantilevered Plates," *Journal of Aircraft*, Vol. 21, No. 1, 1984, pp. 69–76.

[7]Oyibo, G. A., "Generic Approach to Determine Optimum Aeroelastic Characteristics for Composite Forward-Swept-Wing Aircraft," *AIAA Journal*, Vol. 22, No. 1, 1984, pp. 117–123.

[8]Lottati, I., "Flutter and Divergence Aeroelastic Characteristics for Composite Forward Swept Cantilevered Wing," *Journal of Aircraft*, Vol. 22, No. 11, 1985, pp. 1001–1007.

[9]Housner, J. M., and Stein, M., "Flutter Analyses of Swept-Wing Subsonic Aircraft with Parameter Studies of Composite Wings," NASA TND-7539, Sept. 1974.

[10]Librescu, L., and Simovich, J., "General Formulation for the Aeroelastic Divergence of Composite Swept-Forward Wing Structures," *Journal of Aircraft*, Vol. 25, No. 4, 1988, pp. 364–371.

[11]Librescu, L., and Khdeir, A. A., "Aeroelastic Divergence of Sweptforward Composite Wings Including Warping Restraint Effect," *AIAA Journal*, Vol. 26, No. 11, 1988, pp. 1373–1377.

[12]Librescu, L., and Thangjitham, S., "Analytical Studies on Static Aeroelastic Behavior of Forward-Swept Composite Wing Structures," *Journal of Aircraft*, Vol. 28, No. 1, 1991, pp. 151–157.

[13]Karpouzian, G., and Librescu, L., "Comprehensive Model of Anisotropic Composite Aircraft Wings Suitable for Aeroelastic Analysis," *Journal of Aircraft*, Vol. 31, No. 3, 1994, pp. 703–712.

[14]Lee, J., Kim, S.-H., and Miura, H., "Static Aeroelastic Characteristics of a Composite Wing," *Journal of Aircraft*, Vol. 31, No. 6, 1994, pp. 1413–1416.

[15]Petre, A., Stanescu, C., and Librescu, L., "Aeroelastic Divergence of Multicell Wings Taking Their Fixing Restraints into Account," *Revue de Mecanique Appliqueé*, Vol. 19, No. 6, 1961, pp. 689–698.

[16]Oyibo, G. A., "Some Implications of Warping Restraint on the Behavior of Composite Anisotropic Beams," *Journal of Aircraft*, Vol. 26, No. 2, 1989, pp. 187–189.

[17]Oyibo, G. A., and Bentson, J., "Exact Solutions to the Oscillations of Composite Aircraft Wings with Warping Constraint and Elastic Coupling," *AIAA Journal*, Vol. 28, No. 6, 1990, pp. 1075–1081.

[18]Barmby, J. G., Cunningham, H. J., and Garrick, J. E., "Study of Effects of Sweep on the Flutter of Cantilever Wings," NACA Rept. 1014 (supersedes NACA TN 2121), 1951.

[19]Scanlan, R. H., and Rosenbaum, R., *Aircraft Vibration and Flutter*, Dover, New York, 1954.

[20]Librescu, L., *Elastostatics and Kinetics of Anisotropic and Heterogeneous Shell-Type Structures*, Noordhoff International, Leyden, The Netherlands, 1975.

[21]Garber, A. M., "Pyrolitic Materials for Thermal Protection Systems," *Aerospace Engineering*, Jan. 1963, pp. 126–137.

[22]Woods, R. H., "Pyrolitic Graphite for High Pressure, High Temperature Applications," AIAA Paper 76-605, 1976.

[23]Goland, M., "The Flutter of a Uniform Cantilever Wing," *Journal of Applied Mechanics*, Vol. 12, No. 4, 1945, pp. A-198–A-208.

[24]Goland, M., and Luke, Y. L., "The Flutter of a Uniform Wing with Tip Weights," *Journal of Applied Mechanics*, Vol. 15, No. 1, 1948, pp. 13–20.

[25]Peterson, L., *SADSAM User's Manual*, MSR-10, MacNeal–Schwendler Corp., Santa Monica, CA, 1970.

[26]Lehman, L. L., "A Hybrid State Vector Approach to Aeroelastic Analysis," *AIAA Journal*, Vol. 20, No. 10, 1982, pp. 1442–1449.

[27]Librescu, L., Meirovitch, L., and Na, S., "Passive and Adaptive Control of Cantilevered Wing Structures," *10th Symposium on Structural Dynamics and Control* (Blacksburg, VA), edited by L. Meirovitch (to be published).

[28]Librescu, L., and Song, O., "On Static Aeroelastic Tailoring of Composite Aircraft Swept Wings Modelled as Thin-Walled Beam Structures," *Composites Engineering* (Special Issue: Use of Composites in Rotorcraft and Smart Structures), Vol. 2, Nos. 5–7, 1992, pp. 497–512.

[29]Weisshaar, T. A., and Ryan, R. J., "Control of Aeroelastic Instabilities Through Stiffness Cross-Coupling," *Journal of Aircraft*, Vol. 23, No. 2, 1986, pp. 148–155.

[30]Karpouzian, G., and Librescu, L., "Exact Flutter Solution of Advanced Anisotropic Composite Cantilevered Wing Structures," *Proceedings of the AIAA 34th Structures, Structural Dynamics, and Materials Conference*, (La Jolla, CA), AIAA, Washington, DC, 1993, pp. 1961–1966 (AIAA Paper 93-1966).